U. S. Geological Survey.

REPORTS-OPEN FILE SERIES, no. 979: 1968.

NATIONAL AERONAUTICS AND SPACE ADMINISTRATION

EARTH RESOURCES SURVEY PROGRAM

TECHNICAL LETTER NASA-101

THE REMOTE MEASUREMENT OF RHODAMINE B CONCENTRATION WHEN USED AS FLUORESCENT TRACER IN HYDROLOGIC STUDIES

By

H. T. Betts
IIT Research Institute
Chicago, Illinois

January 1968

Prepared by the Geological Survey for the National Aeronautics and Space Administration (NASA) under NASA Contract No. R-146-09-020-006

MANNED SPACECRAFT CENTER
HOUSTON, TEXAS

NR-05-00-000-0101

UNITED STATES
DEPARTMENT OF THE INTERIOR
GEOLOGICAL SURVEY
WASHINGTON, D.C. 20242

Interagency Report
NASA-101
January 1968

Mr. Robert Porter
Acting Program Chief,
Earth Resources Survey
Code SAR - NASA Headquarters
Washington, D.C. 20546

Dear Mr. Porter:

Transmitted herewith is one copy of:

INTERAGENCY REPORT NASA-101

THE REMOTE MEASUREMENT OF RHODAMINE B

CONCENTRATION WHEN USED AS FLUORESCENT TRACER

IN HYDROLOGIC STUDIES*

by

H. T. Betz**

The U.S. Geological Survey has released this report in open files. Copies are available for consultation in the Geological Survey Libraries, 1033 GSA Building, Washington, D.C. 20242; Building 25, Federal Center, Denver, Colorado 80225; 345 Middlefield Road, Menlo Park, California 94025; and 601 E. Cedar Avenue, Flagstaff, Arizona 86001.

Sincerely yours,

William A. Fischer
Research Coordinator
Earth Orbiter Program

*Work performed under NASA Contract No. R-146-09-020-006
**IIT Research Institute, Chicago, Illinois

UNITED STATES

DEPARTMENT OF THE INTERIOR

U. S. GEOLOGICAL SURVEY

Reports - Open file series

INTERAGENCY REPORT NASA-101

THE REMOTE MEASUREMENT OF RHODAMINE B CONCENTRATION WHEN USED AS FLUORESCENT TRACER IN HYDROLOGIC STUDIES *

by

H. T. Betz **

January 1968

This report has not been edited or reviewed
for conformity to Geological Survey standards

Prepared by the Geological Survey
for the National Aeronautics and
Space Administration (NASA)

*Work performed under NASA Contract No. R-146-09-020-006

**IIT Research Institute, Chicago, Illinois

LIST OF FIGURES

LIST OF TABLES

TABLE OF CONTENTS

Technical Memorandum W6137-6

THE REMOTE MEASUREMENT OF RHODAMINE B CONCENTRATION WHEN USED AS FLUORESCENT TRACER IN HYDROLOGIC STUDIES

1. INTRODUCTION

Knowledge of the temporal and spatial distribution of injected fluorescent tracer dyes is useful in determining the movement and dispersion of soluble contaminants in streams, rivers and estuaries. A standard technique involes the injection of a known quantity of dye at a specific location and monitoring the resulting movement and dispersion. Dye concentration is measured with a laboratory fluorometer, and is plotted as a function of distance and time.

Shipborne techniques are relatively slow since samples need to be taken and measured over distances of several kilometers or more. Additionally, the slowly-varying concentrations require repeated or periodic samplings at a given location so that the entire procedure is heavily time consuming. The use of fixed sampling locations, e.g., bridge overpasses, provides precise distance information and virtually continuous records of the time-varying concentration at a fixed site but is highly limited in spatial coverage. Recent efforts towards overcoming

such limitations have employed aerial photography which is analyzed by densitometric measurement in order to relate photographic tone to dye concentration (Ichiye and Plutchak 1966). The photographic technique correlates well with corresponding fluorometer measurements when concentrations are high enough to be visible, estimated at about 50 ppb or more, using rhodamine B dye; fluorometers permit measurements of concentration of the order of 0.1 ppb or less.

This report discusses the possibility of making such measurements by other remote sensors which offer potential improvement in sensitivity over photography. The tracer considered is rhodamine B ($C_{28}H_{31}N_2O_3Cl$) an organic dye which is highly fluorescent at visible (yellow) wavelengths. This dye is cheap, non-toxic in concentrations normally employed, not readily absorbed by stream sediments, and not seriously degraded by light or bacterial action.

2. TECHNICAL DISCUSSION

2.1 Calculation of Radiance of Rhodamine B in Water

In order to determine the possibilities of remotely sensing the concentration of dye in water, it is necessary to determine the emission expected when fluorescence is stimulated by the sun and sky illumination of water containing small quantities of dye.

The emission is calculated as follows:

(1) The specific absorption coefficient of rhodamine B as a function of wavelength is obtained.

(2) Using the values of (1) and the desired concentration and absorption path length of dye, the percentage absorption is calculated as a function of wavelength.

(3) The product of percent absorption and the irradiance of the water surface is obtained and summed over the entire absorption band. (This gives the total flux absorbed by the dye.)

(4) The assumption is made that the quantum efficiency is unity. Then the total number of quanta absorbed is equal to that emitted. Because the two wavelengths of peak absorption and peak emission are fairly close it is assumed that the radiant power emitted is equal to the radiant power absorbed with no correction for wavelength.

(5) The emission curve is obtained for the rhodamine B. From (4) above we will assume that the total power emitted equals that absorbed. From the emission curve we then obtain the fraction of the total power available in any desired spectral band pass.

When the radiant power available in the desired spectral bandpass is known, the signal-to-noise ratio of the detection system can be obtained, provided the background in the spectral bandpass is known. In this case the background is that due to reflection of the sky by the water surface. The direct reflection of the Sun by a smooth surface is completely eliminated by choice of the viewing angle. Since reflection of the Sun by rippled surface cannot readily be estimated, the calculations are made in terms of a smooth surface and a surface in which Sun glitter does not exist. Actual calculations follow.

Figure 1 shows the absorption spectrum of rhodamine B dissolved in alcohol (Poritsky 1924). The water solution is assumed to be identical. This figure shows the measured absolute absorption coefficient for two different concentrations. (The specific absorption coefficient is the same for both curves.) The two concentrations shown are 0.1 gm per 100 cc; and 0.02 gm per 100 cc. The curves are plots of "α" against wavelength where "α" is defined by the equation:

$$\frac{I}{I_0} = 10^{-\alpha x} \qquad (1)$$

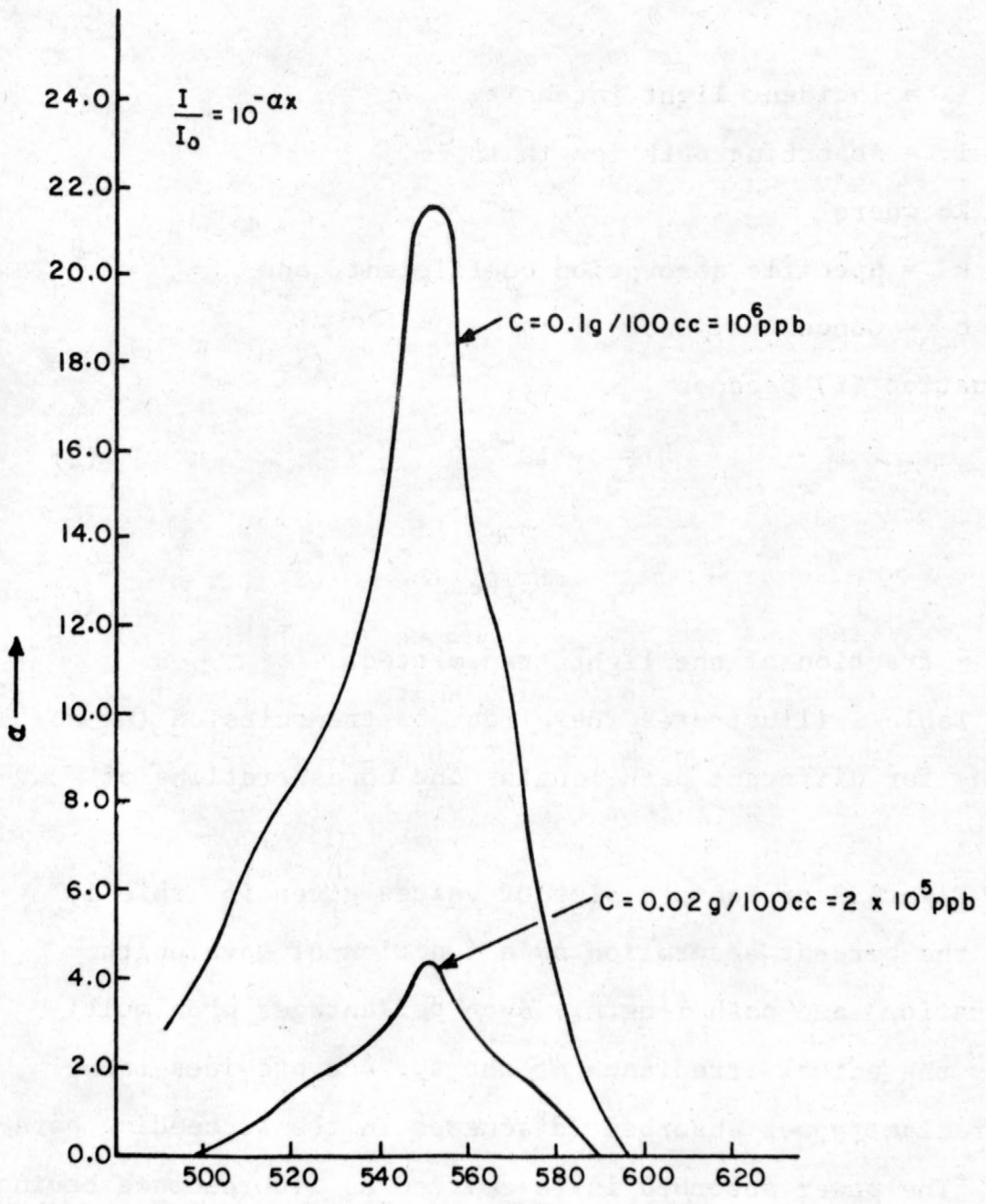

FIGURE I. ABSORPTION COEFFICIENT OF RHODAMINE B

where:

I_0 = Incident light intensity

I = Absorbing path length in cm.

Let α = kc where

k = Specific absorption coefficient, and

c = Concentration.

Then equation (1) becomes

$$\frac{I}{I_0} = 10^{-kcx} \qquad (2)$$

or

$$T = 10^{-kcx} \qquad (3)$$

where T = fraction of the light transmitted.

Table 1 illustrates the effect on transmission (or absorption) for different path lengths and concentrations of interest.

Figure 2 presents a plot of values given in Table 1, showing the percent absorption as a function of wavelength, concentration, and path length. Such percentages when multiplied by the actual irradiance at the surface provides the actual radiant power absorbed (discussed in the succeeding paragraph). The power absorbed is re-emitted as fluorescence having a characteristic spectral distribution illustrated in Figure 3[1]. It is assumed that the emission curve shape does not change

[1]Curve supplied by G. K. Turner Associates. Data was obtained with their Model 210 Spectrofluorometer with a concentration of 200 ppb (by weight).

PERCENT TRANSMISSION AND ABSORPTION OF RHODAMINE B

Wavelength λ	α	1PPB - 10M		30PPB - 1M		30PPB - 10M	
		% Trans.	% Absorb.	% Trans.	% Absorb.	% Trans.	% Absorb.
482	3.0	99.31	0.69	97.95	2.05	81.3	18.7
516	8.0	98.18	1.82	94.62	5.38	57.5	42.5
534	10.8	97.54	2.46	92.81	7.10	47.0	53.0
544	16.0	96.38	3.62	89.54	10.46	33.0	67.0
550	21.6	95.15	4.85	86.14	13.86	22.5	77.5
556	16.0	96.38	3.62	89.54	10.46	33.0	67.0
566	10.8	97.54	2.46	92.81	7.10	46.0	53.0
572	8.0	98.18	1.82	94.62	5.38	57.5	42.5
582	3.0	99.31	0.69	97.95	2.05	81.3	18.7
620	0.0	100.00	0.00	100.00	0.00	100.00	0.0

Values of α were obtained from the Poritsky reference, based on a concentration of 0.1 part rhodamine B in 100 parts of alcohol, where α is defined by the equation: $\log_{10} T = -\alpha x$, where T = transmission.

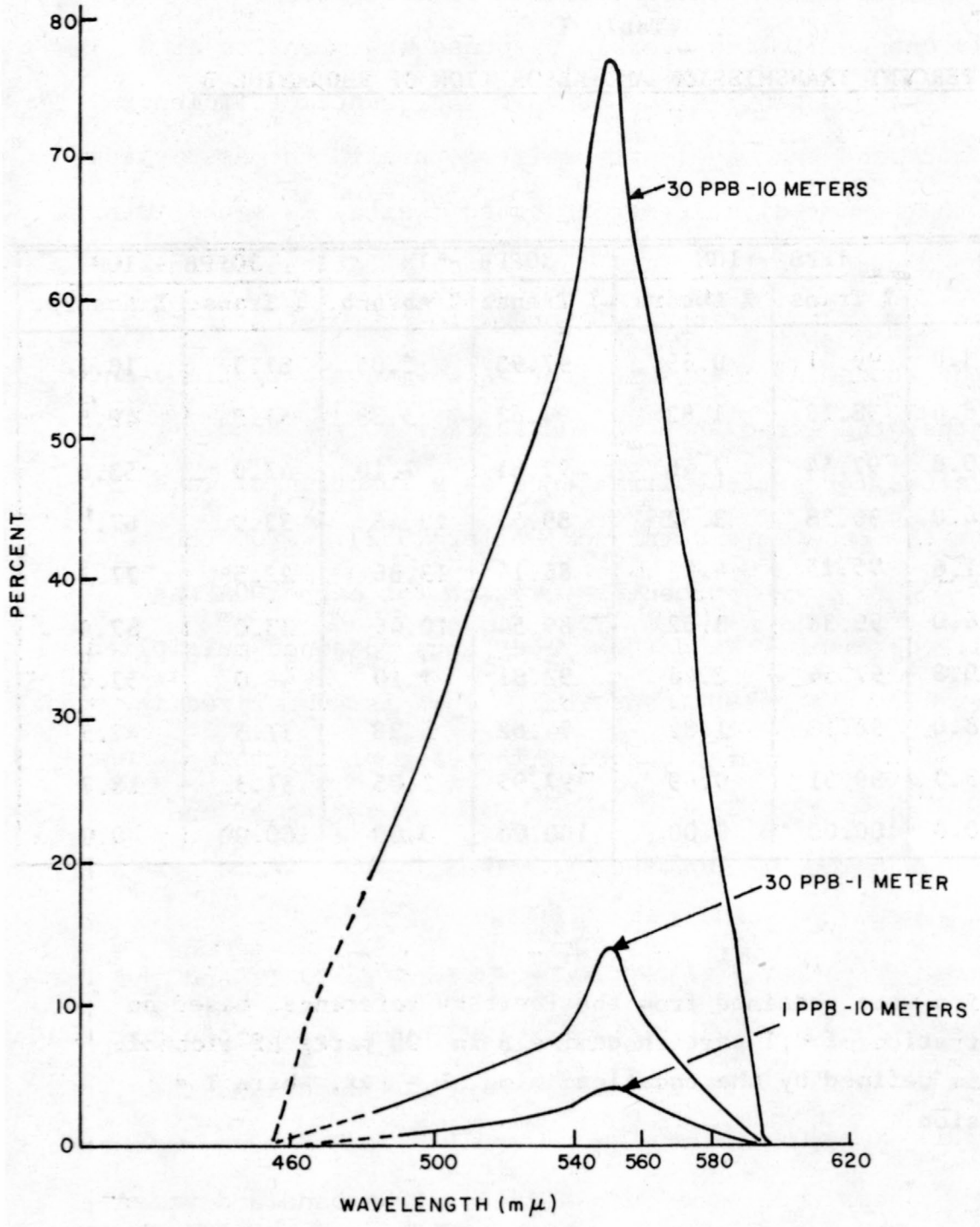

FIGURE 2. PERCENT ABSORPTION FOR VARIOUS CONCENTRATIONS AND PATH LENGTHS OF RHODAMINE B IN WATER

with the amount of incident excitation in its absorption band, but merely changes in its overall response or intensity as a function of wavelength. Also, because the quantum efficiency is near unity and the wavelength shift is small, the assumption was made that the radiant power absorbed (watts) is equal to the power emitted (watts). All further calculations in this report use these assumptions. In order to calculate the radiance of the rhodamine B in water for various concentrations and path lengths, the irradiance on the surface is required.

Values for surface irradiance as a function of wavelength for the Sun, were obtained (Koller 1952). From the curves of Figure 2 the percent absorption for each 100Å was graphically determined, and the values thus obtained multiplied by the irradiance per 100Å bandwidth. This is summarized in Table II. The total power absorbed for each of the three concentrations and path lengths is shown at the bottom of the table. The total power absorbed is given in microwatts per square cm.

Having the total power absorbed from Table II and the emission as a function of wavelength for Figure 3, we can now determine the power emitted in any desired bandpass and the radiance of the surface.

The areas under the curve in each 100Å band and under the entire curve were obtained by graphical integration of Figure 3. The fraction of the power in each 100Å bandpass is then determined by comparing the area in each 100Å band to the

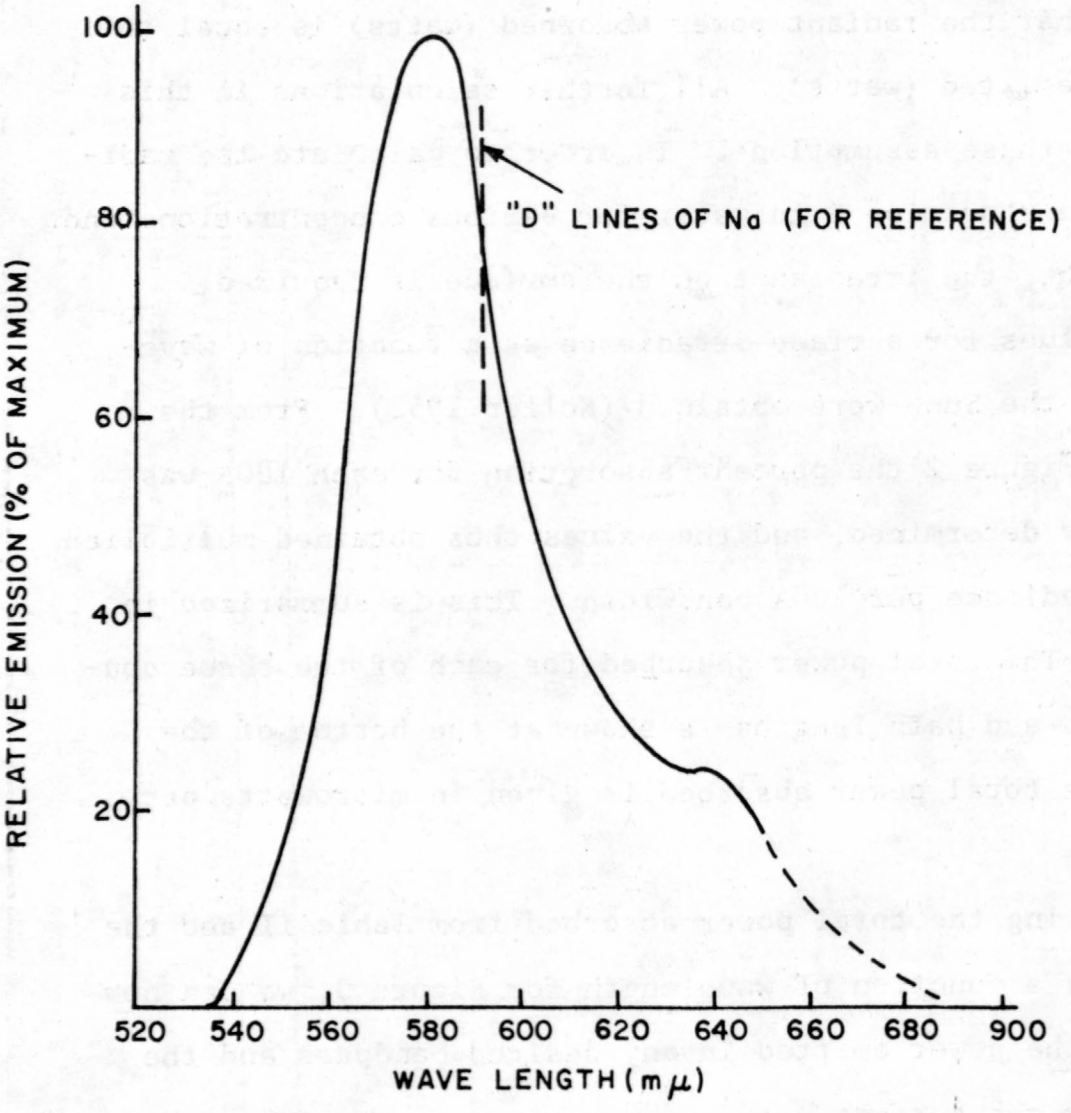

FIGURE 3. EMISSION CURVE OF RHODAMINE B

Table II

POWER ABSORBED BY RHODAMINE B

λ mμ	Total Irradiance Sun & Sky ∘ μ w/cm^2 50A	1PPB - 10 Meters		30PPB - 1 Meter		30PPB - 10 Meters	
		% Absorbed Averaged∘ over 100A	Power Absorbed∘ over 100A μ w/cm^2	% Absorbed over 100Å	Power Absorbed∘ over 100A μ w/cm^2	% Absorbed over 100 Å	Power Absorbed∘ over 100A μ w/cm^2
460	726	0.17	2.46	0.3	4.30	4.5	68.0
470	743	0.45	6.80	1.0	14.86	11.5	171.0
480	743	0.675	10.04	2.5	32.00	17.0	252.6
490	732	1.0	14.64	3.0	43.70	23.5	344.0
500	718	1.25	17.96	3.8	54.50	30.0	430.0
510	692	1.55	21.48	4.8	66.20	38.0	526.0
520	660	1.95	25.72	6.7	89.00	44.5	587.0
530	676	2.25	30.40	6.8	91.80	51.5	696.0
540	793	3.00	47.55	8.5	134.3	60.0	952.0
550	689	4.30	58.40	11.9	164.0	72.0	992.0
560	671	3.00	40.50	8.5	114.0	60.0	805.0
570	663	2.03	26.90	6.2	84.0	45.0	598.0
580	646	1.00	12.92	3.0	38.8	23.5	303.6
590	632	0.30	3.78	0.8	10.5	8.0	101.0
600	621	0.00	0.00	0.00	0.00	0.0	00.0
Total Power Absorbed (μ w/cm^2)			319.55	---	946.80	---	6826.2

* Koller "Ultraviolet Radiation," John Wiley & Sons, 1952, p. 133

area under the entire curve. The values obtained are shown in Table III. The apparent radiance of the water was obtained by assuming that the light is emitted isotropically by the rhodamine B. Hence the surface radiance will be:

$$L = \frac{Wt}{2\pi} \qquad (4)$$

where:

L = radiance of surface

W = total power emitted

t = transmission

The factor "t" is dependent upon the transmission characteristics of the water and the losses due to reflection at the surface. The transmission of the water will depend upon the turbidity and other coloring matter in the water. For clear water the transmission will be unity and is so considered for this report.

The losses due to Fresnel reflection at the surface for zero incidence angle (vertical incidence) amounts to only 2%. There will be a similar loss for the illumination from the Sun and sky but both these factors have been neglected since they are much smaller than the probable error in the original data. The effect of Fresnel reflection is therefore neglected in preparing columns 3 and 4 of Table III. Total internal reflection occurs at the water-air interface for all angles exceeding the critical angle. Refraction at the water air surface causes a change in apparent radiance as the viewing angle departs from

Table III

POWER EMITTED AND APPARENT SURFACE RADIANCE OF RHODAMINE B IN WATER PER 100Å

Wavelength λ mμ	% of Total Power Emitted in 100Å Band	Power Emitted by Rhodamine B μ w/cm²/100Å			Apparent Surface Radiance due to Rhodamine B μw/cm²-ster/100Å			Apparent Surface Radiance due to Fresnel Reflection of Sky μ2/cm²-ster/100Å
		1PPB 10M	30PPB 1M	30PPB 10M	1PPB 10M	30PPB 1M	30PPB 10M	
540	0.0	0.0	0.0	0.0	0.0	0.0	0.0	2.02
550	2.8	8.9	26.5	191.0	1.4	4.2	34.4	1.96
560	8.0	25.6	75.7	546.0	4.1	12.1	87.0	1.87
570	17.8	56.8	168.5	1354.0	9.1	26.8	195.0	1.76
580	19.8	63.4	187.5	2160.0	10.1	29.8	215.0	1.68
590	15.0	47.9	142.0	1024.0	7.6	22.6	166.0	1.58
600	10.5	33.6	99.4	716.0	5.3	15.8	114.0	1.51
610	6.2	19.8	58.7	427.0	3.2	9.3	67.4	1.44
620	5.5	17.5	52.0	376.0	2.8	8.3	59.8	1.40
630	4.8	15.3	45.4	328.0	2.4	7.2	52.2	1.36
640	4.8	15.3	45.4	328.0	2.4	7.2	52.2	1.30
650	3.4	10.8	32.2	232.0	1.7	5.1	37.0	1.23
660	1.5	4.8	14.2	102.0	0.8	2.3	16.6	1.18
670	0.5	1.6	4.7	34.0	0.3	0.8	5.4	1.17
680	0.0	0.0	0.0	0.0	0.0	0.0	0.0	1.16

the vertical. However, for vertical viewing, the radiance is the same as if there were no interface. Columns 3 and 4, therefore, indicate radiance for vertical viewing neglecting Fresnel losses.

The radiance of the rhodamine B will be seen against a background radiance due to the reflection of the sky in the water surface, that is, the apparent radiance of the sky as reflected in the water surface. This will be Fresnel reflectance at the surface and for vertical viewing the reflected radiance of the surface will be 2% of the sky radiance, with a spectral distribution identical to that of the sky. Column 5 of Table III was calculated using the irradiance of the surface from Reference 2, and assuming the sky to be completely uniform in brightness over the entire hemisphere. (It is usually brighter at the horizon so this assumption for vertical viewing will give a slightly high value.)

It should be noted that under the ideal conditions of clean water and clear unrippled surface here assumed that there will be neither specular or diffuse reflectance of the Sun. The only background radiance will be that due to Fresnel reflectance of the sky. Diffuse reflectance of the area due to rippled surfaces, turbid water, or a dirty surface can be evaluated only in the practical case by experimental measurement.

2.2 Photographic Detection of Rhodamine B in Water

Recent measurements of rhodamine B concentrations in sea water by aerial photography (Ichiye and Plutchak 1966),

offer a preliminary basis for evaluating this remote sensor approach to such dye tracing.

The sea was photographed through a suitable filter chosen so as to enhance the contrast between the dye patches and the general sea background. The dye areas appear as areas of greater radiance than that of the reflected sky. A microdensitometer is used to evaluate the exposure on the film and from this the vertically integrated amount of dye present is determined. The vertical profile cannot be determined by this technique but requires an additional sampling in depth from surface craft located in the area. In addition, corrections for water color and turbidity must be made.

In practice the areas desired were scanned along a line by the densitometer and recordings made. The photographs (and also the densitometer traces) show the effects of the reflection of the Sun by waves. This "Sun glitter" poses no particular problem since the curves are smoothed by eye in which the high spikes on the microdensitometer traces are merely ignored; such smoothing may apply to other remote sensor techniques exhibiting spike anomalies in their data.

The photographs in the Ichiye and Plutchak reference were made with the following conditions:

Filter	Wratten 23A
Lens aperture	F/8
Exposure time	1/400 sec
Film type	Tri.-X Aerecon
Film speed	ASA 200 Kodak Data Sheet

Film sensitivity Density 1 0.1 erg/cm^2
Density .3 0.027 erg/cm^2

To get some idea of the sensitivity of the photographic method, the exposures resulting from the apparent surface radiances for various concentrations of dye are calculated. The transmission of the Wratten 23A filter (Kodak Wratten Filter Manual, 19th ed.) as a function of wavelength was multiplied by the corresponding radiances of the various dye concentrations of Table III and summed to give the total effective radiance for each concentration. A similar total effective radiance was calculated for the reflected sky through the 23A filter. This is summarized below:

Effective Radiance (10PPB-10 meter) = 26.4 μwatts/cm^2-ster

Effective Radiance (30PPB- 1 meter) = 80.9 μwatts/cm^2-ster

Effective Radiance (30PPB-10 meter) = 622.8 μwatts/cm^2-ster

Effective Radiance of Reflected Sky = 11.4 μwatts/cm^2-ster

The exposure of the film expressed in erg/cm^2 is given by:

$$E = L\Omega t \times 10^7$$

where:

L = effective radiance of the source

Ω = solid angle of collection

t = time of exposure

Substituting the values for radiance of the various concentrations and reflected sky background, the solid angle (1.22×10^{-2} steradian) for an F/8 system, and an exposure time t = 1/400 sec., one obtains:

a) $E_{10PPB\text{-}10\ meter} = (26.4 + 11.4)\ (10^{1})\ (1.22 \times 10^{-2})\ (1/400)$

$= 0.015\ ergs/cm^2$

b) $E_{30PPB\text{-}\ 1\ meter} = 0.029\ ergs/cm^2$

c) $E_{30PPB\text{-}10\ meter} = 0.193\ ergs/cm^2$

d) $E_{Reflected\ Sky} = 0.0035\ ergs/cm^2$

Reference to the Kodak Data Sheet for Tri-X Aerocon film indicates the following image densities for these exposures:

a) Approximately 0.2 density units above fog for 1PPB concentration having a 10 meter depth.

b) Approximately 0.3 density units above fog for 30PPB concentration having a 1 meter depth.

c) Approximately 1.1 density units above fog for 30PPB concentration having a 10 meter depth.

d) Exposure to the reflected sky background will be lost in the gross fog level of the film.

The possibility of detection of rhodamine B dye in water is clearly demonstrated for concentration of the order of 30PPB at a depth of 10M. (That is, dye concentation constant from the surface down to a depth of 10M, below which there is no dye.) The remaining two conditions of concentration, 30PPB-1 meter and 1PPB-10 meters, are somewhat marginal in that both produce densities which lie in the toe region of the film characteristic curve; it should be noted that the 1PPB case differs only by a factor of about 2 in exposure over the "noise" background. The contrast capability of the photographic approach indicated by these calculations will be degraded under less idealistic

assumptions. For example, under conditions which tend to absorb or scatter the exciting and/or fluorescent radiation, e.g., turbid waters, the effective dye emission will be reduced. Similarly, where the water surface is non-planar or agitated or wavy the skylight reflection may be increased considerably beyond the two percent assumed in these calculations. Factors which reduce the emitted fluorescence or increase the surface reflections, or both, will degrade the contrast anticipated from the calculations performed. Additionally, conditions involving overcast skies have not been treated at this writing.

It is difficult to compare these idealistic results with actual values obtained by experiment, since the turbidity of the water was neglected; however, detection which is in good qualitative agreement has been achieved for concentration of 30-50 PPB in the rather turbid water of Long Island.

The photographic method of measurement of dye concentration in sea water appears to be a very practical approach, especially when lateral distribution is desired, for concentrations of about 30 PPB or more.

2.3 Detection of Rhodamine B by "Line Depth" Method

2.3.1 Theory of Measurement

The Fraunhofer line-depth technique has been used by Kopal and others to measure the luminescence of the lunar surface (Kopal 1960). It may readily be applied to the measurement of luminescence which is excited by the sun and is measured in the presence of scattered or reflected sunlight.

ment of fluorescent tracers as well as other luminescent materials on the Earth's surface, from aircraft or satellites (USGS Technical Letter, NASA-70, 1966).

The determination of luminescence by the method of line depth is based on observable changes in the spectral profiles of Fraunhofer lines obtained from a surface which reflects and is also excited to luminescence. The principle is illustrated in Figure 4, which presents idealized line profiles in which the finer structure or variations have been removed. Absorptions in the solar atmosphere provide a number of Fraunhofer lines which are useful for determination of surface luminescence (Table 4). Non-luminescent materials reflect profiles whose R_s ratios are identical to that measurable for the incident solar radiation. Materials which luminesce exhibit higher ratios, i.e., R_t R_s. A <u>relative</u> measure of luminescence is expressible in terms of two profile measurements which provide R_s and R_t, and is given by:

$$\rho = \frac{I_\ell}{A} = \frac{R_t - R_s}{1 - R_t} \qquad (5)$$

Since $D = A + I_\ell$, Figure 4C, one can modify the relative luminescence expression of equation (5) to provide the absolute intensity of luminescence explicitly, as

$$I_\ell = \left(\frac{P}{1+\rho}\right) D \qquad (6)$$

where ρ and D are measurable from the output record.

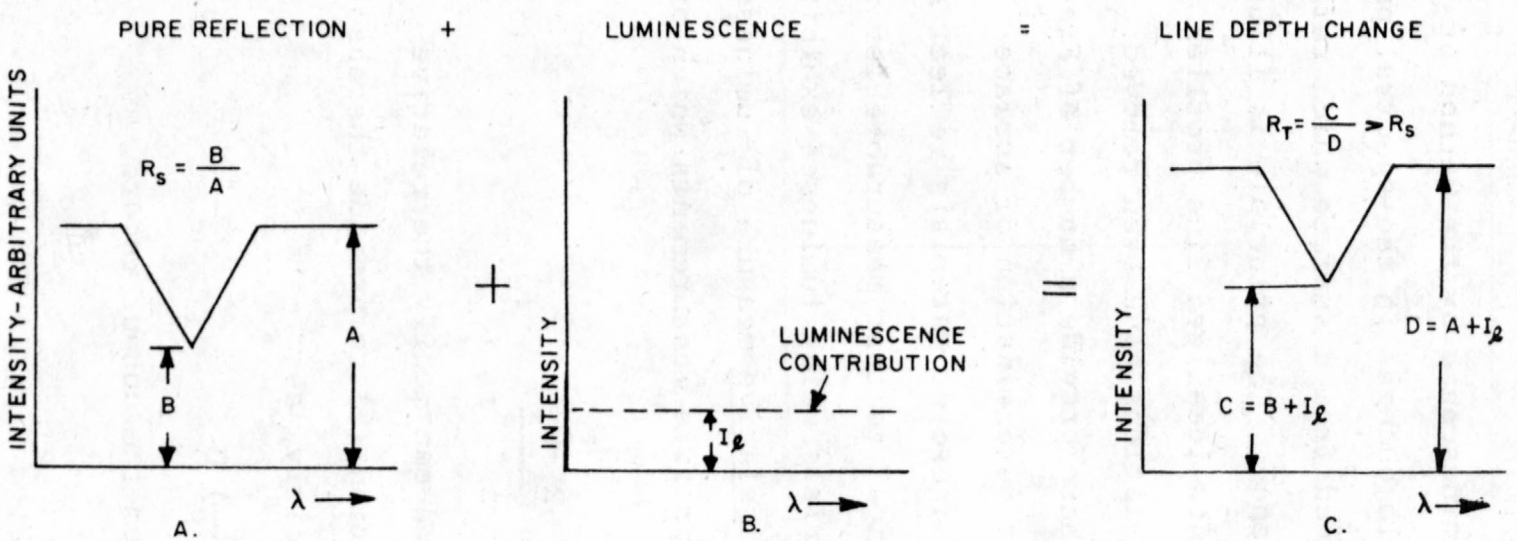

A. IDEALIZED LINE PROFILE FROM INCIDENT SUNLIGHT. NON-LUMINESCENT SAMPLES REFLECT SUCH PROFILES (SAME R_S) WITH REDUCED INTENSITY. CONCEPTUALLY, THE PURELY REFLECTED COMPONENT FROM LUMINESCENT SAMPLES WOULD EXHIBIT THE SAME R_S.

B. LUMINESCENCE SPECTRUM IS ESSENTIALLY FLAT OVER THE NARROW BAND MEASURED.

C. RESULTANT PROFILE FROM SAMPLE WHICH REFLECTS AND LUMINESCES. EVIDENCE NOTED BY MEASUREMENT OF HIGHER R RATIOS COMPARED TO THAT OF INCIDENT SUNLIGHT.

FIGURE 4. PRINCIPLE OF FRAUNHOFER LINE DEPTH METHOD

Table IV

FRAUNHOFER LINES IN THE NEAR ULTRAVIOLET AND VISIBLE REGIONS OF THE SPECTRUM, SUITABLE FOR OBSERVATION BY THE LINE DEPTH METHOD

Line	Color	Wavelength	Source
C	Red-orange	6563 Å	Hydrogen
D_1	Yellow	5896 Å	Sodium*
D_2	Yellow	5890 Å	Sodium*
F	Blue	4861 Å	Hydrogen
G	Violet	4340 Å	Hydrogen
H	Deep violet	3968 Å	Calcium
K	Deep violet	3934 Å	Calcium

* These lines appear applicable for the measurement of luminescence involving the rhodamine B tracer which fluoresces over a 5600-6000Å band (~half-power response points).

The ratio R_s, is obtainable by (a) spectrally scanning across the Fraunhofer line collected directly from the sun and determining the null-to-shoulder intensity ratio, or (b) performing the measurement from radiation that is reflected from a known non-luminescent material under solar illumination, or (c) using two fixed narrow band filters, spectrally located at the null and shoulder regions respectively, instead of the spectral scan for (a) or (b) above. R_t is obtained in a manner identical to that given for R_s except that the reflected line profile is measured from the suspect luminescent surface. Thus, in computing the relative luminescence value, using equation (5), one uses only the measured ratios for R_t and R_s and absolute calibration is not involved. To obtain the absolute intensity of luminescence, using equation (6), one must calibrate the instrument response in order to convert the recorded output for D into its equivalent absolute input.

Examination of the line-depth relationships, Figure 4, indicates that this technique is more applicable for conditions of relatively low tracer concentrations or luminescence intensities than for high rhodamine B concentrations. This is shown by examining the measurable change in R_t (Figure 4) with change in the amount of luminescence, I_ℓ. Since

$$R_t = \frac{B + I_\ell}{A + I_\ell} \tag{7}$$

then, for small changes in I_ℓ,

$$\Delta R_t = \frac{1}{(A+I_\ell)} \left[1 - \frac{(B+I_\ell)}{(A+I_\ell)} \right] \Delta I_\ell \qquad (8)$$

For dye concentrations greater than 30PPB,

$$I_\ell \gg A > B \qquad (9)$$

so that the term inside the bracket, Eq. 8, is essentially zero, indicating that R_t would exhibit a negligible change as I_ℓ changes.

In contrast to this effect for high luminescence emission conditions, the method becomes much more practical for low concentrations. When

$$I_\ell \ll B < A \qquad (10)$$

then

$$\Delta R_t = \frac{1}{(A)} \left[1 - R_s \right] \Delta I_\ell \qquad (11)$$

Equation (11) indicates that R_t will change proportionately to a given change in luminescence. It is important to note also that sensitivity to luminescence change, ΔI_ℓ, depends on the magnitude of the $(1-R_s)$ coefficient which depends on the degree of spectral resolution employed in measuring A and B; poor spectral resolution with respect to the Fraunhofer line width (e.g., $\sim$1Å for the sodium D line) will result in relatively high measured values of R_s (B/A) which, in turn, provides a small $(1-R_s)$ coefficient, Eq. 11, and reduces the rate of change of ρ with luminescence.

Specific calculations involving rhodamine B concentrations are discussed in Section 2.3.2 for line-depth technique.

lunar case, where the sunlight is fairly uniformly scattered, the factor ρ is a good measure of the relative luminescence between sample areas of such surfaces. Equation (5) illustrates this point. If the purely reflected shoulder intensity, A, remains practically constant from sample to sample area, than ρ is directly proportional to the absolute intensity of luminescence from each area, I_{ℓ}. If, however, the amount of light reflected (or scattered) to the remote detector is a strong function of viewing angle, e.g., under specular glitter conditions as opposed to diffuse reflections, then the apparent luminescence will be a function of surface orientations. This can introduce undesirable ambiguities in comparing the relative luminescence between sample areas. In view of the potential enhancement of sensitivity offered by the line depth method (Section 2.3.2) to rhodamine B concentration measurement, the specular glitter problem deserves further discussion.

Repeating Eq. (5) for convenience,

$$\rho = \frac{I_{\ell}}{A} = \frac{R_t - R_s}{1 - R_t} \qquad (5)$$

one can note the effect on ρ as the reflected shoulder intensity A, becomes large under glitter conditions. First, ρ values derived by measurement will approach zero (or the instrument noise level) as A is significantly increased, assuming the luminescence, I_{ℓ}, remains constant. Second, the ability to discriminate between patches having different dye concentrations (or I values) will be reduced since,

$$\Delta\rho = \frac{1}{A}\Delta I_{\ell} \qquad (12)$$

and 1/A presents a small coefficient as A becomes significantly large. Third, assuming luminescence constant over an area, any localized high reflectivity conditions will exhibit sharply lowered ρ values so that the absolute value of ρ is affected by such conditions. One can compensate for such absolute errors by appropriate processing of the measured A-B-C-D values.[2]

There are several possibilities for minimizing the effect of specular reflections from rippled water surfaces under sunlit excitation. One approach to this problem might utilize the line depth sensor whose acceptance beam is oriented from the vertical such that reception of specularly reflected rays is minimized. Figure 5 illustrates the dispersion of rays from a rippled surface approximated by a sinusoidal cross-section. This idealized geometry indicates that the specularly reflected rays are confined to specific limits in angle from the vertical, which depend on the ripple amplitude, A, and wavelength, λ, and solar elevation angle, $\emptyset$; Appendix A discusses the derivation of limits. In view of such limiting angles, one can tilt the remote sensor acceptance beam to minimize reception of such rays. For example, consider a rippled surface approximated by a wave amplitude of 0.5 inch and wavelength of 4 inches with a solar elevation of 40°. The specular

[2] H. Goldman, IITRI, "Review of the Perkin-Elmer Design for the FLD," Memorandum to the USGS (W. Hemphill), October 10, 1967.

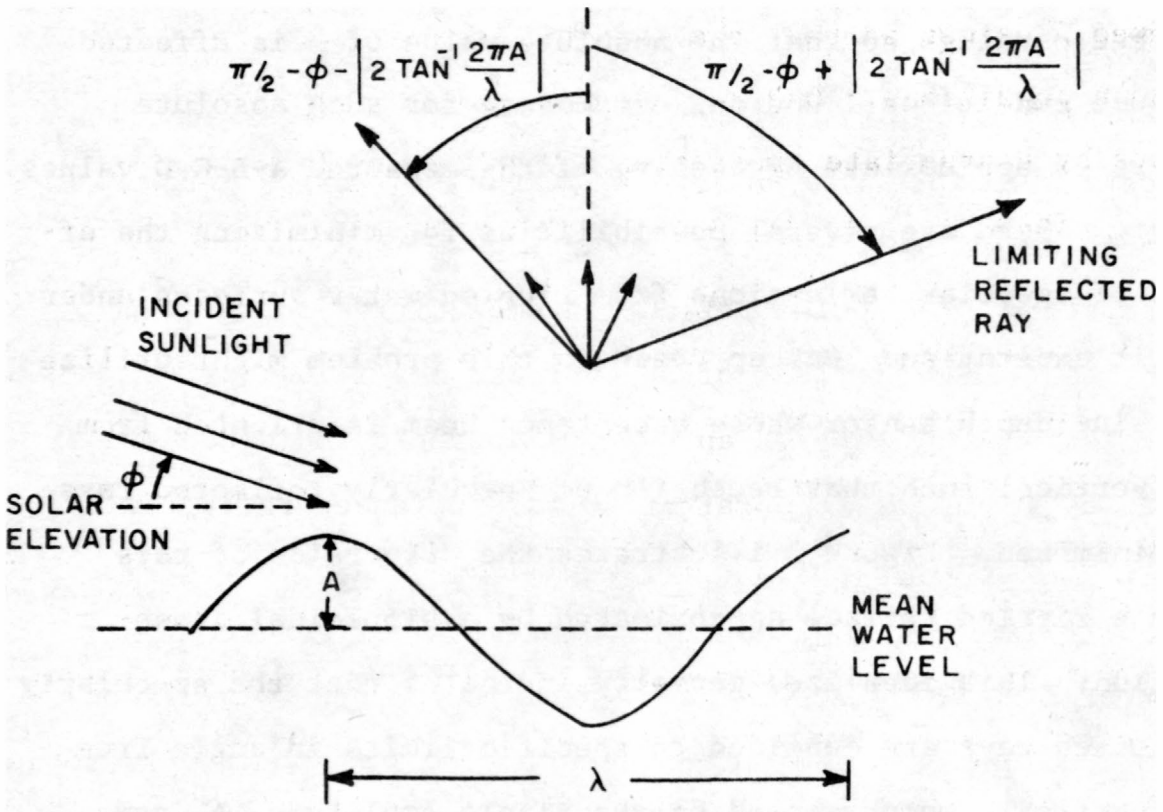

FIGURE 5. SPECULAR REFLECTION GEOMETRY FOR SINUSOIDAL RIPPLE

rays are scattered between about 26° from the vertical towards the sun to about 90° from the vertical away from the sun (see Figure 5). If the instrument were tilted (in the plane of the figure) such that the beam acceptance angles were, say between 35° and 45° from the vertical, away from the sun's direction, reception of the specular glitter would be heavily reduced. While this example is limited in conditions assumed, it illustrates a principle that could reduce the ambiguity introduced by specular glitter. Another condition which should deny the introduction of specular reflection ambiguities in the line depth measurement is that of an overcast sky illumination. In this case one anticipates an almost isotropic incidence of radiation resulting in a rather uniform diffused reflectivity.

A third possibility for minimizing the potential ambiguity introduced by specular glitter of direct sunlight, might utilize the discounting of anomalous or sharply-discontinuous values measured during overflight; this would correspond to eliminating small bright spots in the photographic method as being glitter in the image recorded. Since the line-depth method integrates all energy received from relatively large areas of resolution (1° acceptance at 6000 ft. altitude corresponds to about a 100 x 100 ft. area), one anticipates that the concentration to be measured along the flight path would exhibit a relatively smooth variation. By incorporating the tilted beam technique such as suggested previously to reduce

glitter, any sharp changes in measured ρ (or I_ℓ) values would be indicative of inadequate glitter rejection.

Finally, and perhaps the simplest approach to eliminating glitter effects, is selection of the flight path which exhibits the least amount of specular reflection. A pilot's visual observation of the water surface for several different directions of flight may suffice for selection of flight path. For example, under a fairly uniform water wave condition, a flight path parallel to the wave troughs should remove much of the glitter reflected to the instrument.

2.3.2 Use of the Fabry-Perot Interferometer in Line-Depth Measurement of Rhodamine B

A Fabry-Perot interferometer may be used as a photoelectric spectrometer to measure the line depth of the areas of sea containing rhodamine B as a tracer dye. This device uses the multiple reflections between parallel surfaces spaced so as to create reinforcement or constructive interference of a specified narrow band of incident radiation which is then detected by a photomultiplier. By periodically varying the plate spacing, the narrow line spectrum can be repeatedly scanned to determine the line depth ratios. Table V presents characteristics of such an interferometer for use with a sodium D line which would be very suitable for the rhodamine B luminescence. The interferometer could be mounted in an aircraft to look vertically or tilted off vertical such as suggested in Section 2.3.1 to reduce glitter ambiguity.

Table V

CHARACTERISTICS OF INTERFEROMETER SPECTROMETER
FOR USE WITH Na "D" LINES

Forefilter width at 1/2 maximum	4Å
Interferometer free spectral range	5Å
Interferometer spectral bandpass	0.25Å
Total angular field	1° 4'
Solid angle of acceptance	2.67×10^{-4} ster.
Transmission efficiency of interferometer	60%
Plate separation	.35mm
Area of interferometer plates	5 cm^2
Multiplier phototube type	S-20
Cathode sensitivity of phototube	.07 A/watt

The signal-to-noise ratio of this system is calculated as follows: the noise current generated in a multiplier phototube due to the random emission of photoelectrons at the cathode (Zworykin and Ramberg 1950) is:

$$\text{Noise} = \sqrt{2\ e\ i\ \Delta F} \tag{13}$$

where e = the charge of the electron

i = the cathode current of the multiplier

ΔF = the frequency bandwidth of the electronic signal generated.

The signal-to-noise current ratio is therefore

$$\frac{\text{Signal}}{\text{Noise}} = \frac{\text{Cathode Signal Current}}{\sqrt{2e\ (\text{total cathode current})\ \Delta f}} \tag{14}$$

The radiant power on the multiplier phototube is

$W = L\Omega AT\Delta\lambda$

L = radiance of the source in $(W/cm^2\text{-ster}/\mathring{A})$

Ω = solid angle of acceptance of the interferometer

A = area of the interferometer (cm^2)

T = transmission of the interferometer

$\Delta\lambda$ = spectral bandpass

Δf = frequency bandwidth

The cathode current is:

$i = WS$, where

S = sensitivity of cathode in amp/watt.

The expression for signal-to-noise ratio may be written:

$$\frac{\text{Signal}}{\text{Noise}} = \frac{L_S}{\sqrt{\Delta f}} \sqrt{\frac{T\Omega AS\Delta\lambda}{32 \times 10^{-20}(L_S+L_B)}} \qquad (15)$$

where L_S = radiance due to rhodamine B

L_B = radiance due to sky background.

Substituting in the above equation the values for radiance at 5900Å of various concentration of rhodamine B and the values for sky radiance from Table III, one obtains the signal-to-noise ratios for an S-20 photocathode. The noise contribution due to the background (reflected sky) is negligible-themain noise contribution being essentially "the noise in signal" due to the random emission of photoelectrons at the cathode. Similarly, the change in noise from the wing to center of the Fraunhofer line is small and may be neglected except where only the sky background is considered, i.e., lines 4 and 5 of Table VI.

The effect of various concentrations of dye on the "depth" of the Fraunhofer "D" lines can be computed. (By line "depth" is meant the ratio of the center (minimum) to the wing (maximum) for the line.) Two cases are considered. Case I involves background reflection due to that of the sky only (as shown in Table VI) and Case II considers conditions where the sun is reflected by the water waves (characterized as "sun-glitter"); this condition was introducted in Section 2.3.1.

VALUES OF SIGNAL-TO-NOISE FOR VARIOUS CONCENTRATIONS OF RHODAMINE B IN SEA WATER USING FABRY-PEROT INTERFEROMETER

Conc. & Path Length of Rhodamine B	Spectral Radiance[1] W/cm^2-sterÅ at 5900Å	Radiance[2] W/cm^2-ster .25Å at 5900Å	Signal-to-Noise Ratio[2] S/N
1PPB-10M	7.6×10^{-8}	1.9×10^{-8}	$\frac{16.2 \times 10^2}{\sqrt{\Delta f}}$
30PPB-1M	22.6×10^{-8}	5.65×10^{-8}	$\frac{30.4 \times 10^2}{\sqrt{\Delta f}}$
30PPB-10M	166×10^{-8}	41.6×10^{-8}	$\frac{86 \times 10^2}{\sqrt{\Delta f}}$
Reflected Sky Wing (no dye)	1.6×10^{-8}	4×10^{-9}	$\frac{8.6 \times 10^2}{\sqrt{\Delta f}}$
Reflected Sky Center (no dye) 13% viz.	2.08×10^{-9}	5.2×10^{-10}	$\frac{3.1 \times 10^2}{\sqrt{\Delta f}}$
Reflected Sun Wing of Line	1.15×10^{-3}	2.88×10^{-4}	
Reflected Sun Center of Line	1.49×10^{-4}	3.74×10^{-5}	

1. Values from Table III
2. Calculations based on S-20 multiplier and interferometer in Table IV.

$$R_S = \frac{\text{Radiance of center for background}}{\text{Radiance of wing for background}} = .13$$

and is the same as for the sun observed directly.

The values of R_T depend upon the radiance of the dye for various concentrations and upon the reflected sky radiance. It is expressed in general as:

$$R_T = \frac{\text{Radiance due to dye + Radiance of sky at line center}}{\text{Radiance due to dye + Radiance of sky at wing of line}}$$

Solving this for the various concentrations gives:

For IPPB-10M

$$R_T = \frac{1.9 \times 10^{-8} + 5.2 \times 10^{-10}}{1.9 \times 10^{-8} + 4 \times 10^{-9}} = .85$$

For 30PPB-1M

$$R_T = .9425$$

For 30PPB-10M

$$R_T = .99163$$

Calculating ρ from Eq. (5)

For 1PPB -10M ρ = 4.75 = 475%
For 30PPB-1M ρ = 14.13 = 1413%
For 30PPB-10M ρ =103.00 = 10300%

Although the above calculations for ρ indicate clearly discerned differences in value with gross changes in concentration conditions, one needs to examine these with some reservation when the actual measurables are considered. In practice, one processes the data to determine the R_T ratio and then ρ is derived from the latter (and R_S). Therefore, one should

examine changes with luminescence of the more fundamental measurable, R_T, for more meaningful evaluation of the technique; note that the range of variation for the estimated R_T values given above is only about 99/85 or less than 1.2, whereas the variation of the derived ρ values exceeds 21. Assuming a 20% reduction in luminescence for each of the three concentrations assumed, one obtains:

For (1PPB-δ)/10M

$$R_T' = .819$$

$$\frac{\Delta R_T}{R_T} \approx 4\% \text{ change in actual measurable}$$

For (30PPB-δ)/1M

$$R_T' = .929$$

$$\frac{\Delta R}{R_T} \approx 1.4\% \text{ change in actual measurable}$$

For (30PPB-δ)/10M

$$R_T' = .98991$$

$$\frac{\Delta R}{R_T} < 0.2\% \text{ change in actual measurable}$$

These computations clearly point to the better utility of the line depth method for relatively low concentrations as opposed to the 30PPB case, where the system offers a "saturated" result. In this connection, it is noted that the line depth method has had considerable success in lunar observation where rock luminescence exhibited ρ values of 5% (Grainger and Ring 1962) in

contrast to high values computed for the intense rhodamine B emissions considered in this study.

In summary, for very low concentrations of dye, where the radiance of the dye is of the same order as the scattered sky radiance or smaller, the Fraunhofer line depth measurement becomes significant, and should be especially useful for very small amounts of dye. If the background is high due to suspended particles in the water, the Fraunhofer line depth method would also be useful. It would in general be useful whenever the luminescence L is less than 100% of the scattered background radiation. In any application, however, a measurement of the surface irradiance is recommended for comparison with the measurement for luminescence, I_ℓ, of Figure 4.

Case II: Effect of Reflectance of Sun by Water Waves

The direct (specular) reflectance of the sun into the airborne line depth interferometer, will exhibit extremely high intensity values for A and B as shown in the two bottom lines of Table VI. (based on a 2% reflection coefficient). These intensity values are about 2 to 4 orders of magnitude larger than those estimated from the rhodamine B concentrations which have been considered. If one applies this condition of $A \gg I_\ell$ and $B \gg I_\ell$ to Eq. (7) given in Section 2.3.1, it is readily apparent that the measured R_T value is close to that of a non-luminescent reflector, or

essentially equal to $R_s = \frac{B}{A}$. Actual calculation of the three concentration conditions are presented below to illustrate this point:

For 1 PPB-10M

$R_T = .13 + 55.5 \times 10^{-5}$ or a change of .05% from the R_s value exhibited by a non-luminescent surface.

For 30PPB-1M

$R_T = .13 + 1.96 \times 10^{-4}$ or a change of 0.15%

For 30PPB-10M

$R_T = .13 + 1.4 \times 10^{-3}$ or a change of 1.1%.

In summary, unless extremely high concentrations of dye are of interest, the line depth method fails to discriminate between various concentrations if the background is high due to direct reflection of sunlight.

2.4 Filter Photometer for the Detection of Rhodamine B in Water

Another method of detection might be to use a simple filter photometer. A schematic diagram of a simple photometer is shown in Figure 5a. It consists of an interference filter, a lens and aperture for defining the desired angular field of view, and a detector. The instrument would be scanned over the field of interest and the radiance recorded. An exactly similar instrument, bore-sighted so as to cover the identical field of view, would be used to measure the light reflected in a spectral region where no fluorescence appears. The band passes of the

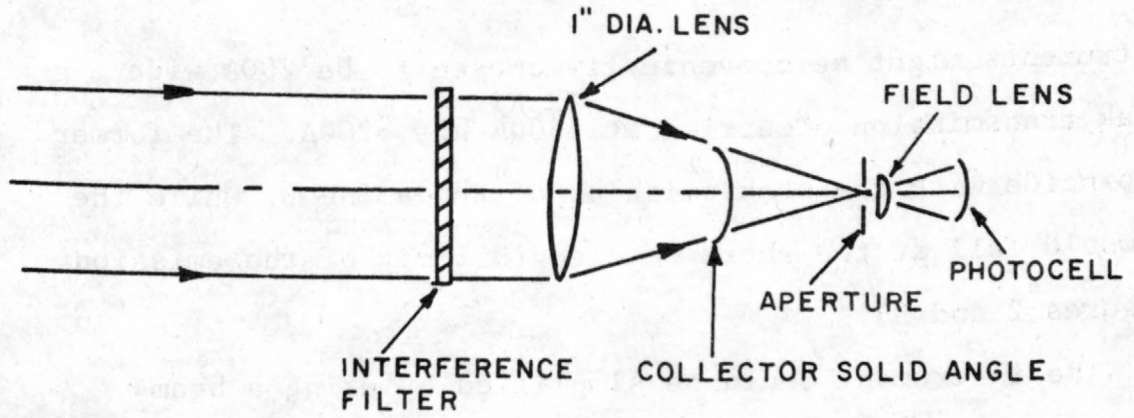

(A)

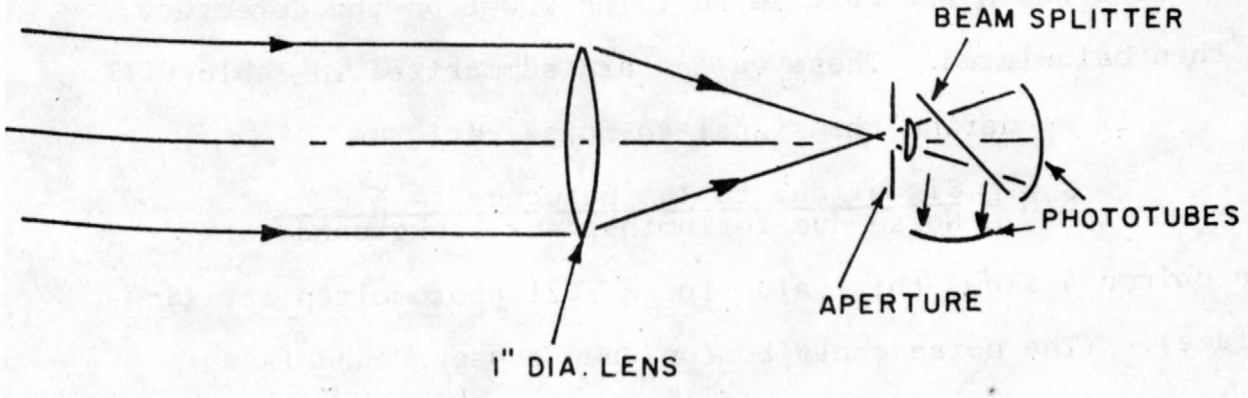

(B)

FIGURE 6. SCHEMATIC DIAGRAM OF FILTER PHOTOMETER

two instruments might be conveniently chosen to be 200Å wide with peak transmission occurring at 5800Å and 5200Å. The former would coincide with the peak emission of rhodamine B, while the latter would fall at the short wavelength limit of the emission (see Figures 2 and 3).

The instrument could be simplified by using a beam-splitter and two filters and two detectors so as to use the same collecting lens and aperture (Figure 5b). If a dichroic beam-splitter is used, very little additional light loss would result from the combined system over the separate photometers.

The characteristics of a typical instrument are shown in Table VII.

By referring to Table III the effective radiances for a 200Å band width are calculated. The power on the detector was then calculated. These values are summarized in Table VIII.

If we define the signal-to-noise ratio as

$$S/N = \frac{\text{Signal due to luminescence}}{\text{Noise due to luminescent background}}$$

then column 4 shows this value for a 1P21 photomultiplier (S-4 surface). (The noise contribution due to background is so small that is may be neglected except for lines 4 and 5.)

Suppose an aircraft traveling at 140 miles per hour at an altitude of 1,000 ft. scans the area with an instrument as described, pointed vertically downward. The time required to cover one degree (2 x 17.5 ft.) on the ground is 0.153 sec. For estimating signal-to-noise we may assume a dwell time of 0.153

Table VII

DUAL FILTER PHOTOMETER CHARACTERISTICS

Lens diameter	2.54 cm
Lens area	5.1 cm^2
Focal length	10.16 cm
F number	F/4
Collector solid angle	4.8×10^{-2} sterad.
Aperture diameter	.18 cm
Aperture area "a"	$2.5 \times 10^{-2} cm^2$
Total field angle	1°
Filter #1	
Width at 1/2 max.	200A
Centered at	5800A
Filter #2	
Width at 1/2 max	200A
Centered at	5200A
Transmission of system (for each channel)	50%

sec. or a corresponding Δf of 6.5. These values are shown in column 5 of Table VIII. It is to be noted that these values of S/N are very large and could be safely reduced by using a smaller field of view, while using the same objective, with a correspondingly shorter dwell time, thus giving greater area resolution on the ground.

The technique of evaluating luminescence would be to compare the signal from the background at 5200Å to the values at 5800Å. The value of background at 5200Å is essentially representative of the value of the background at 5800Å. (That is, the background at 5800 due to sky is approximately .85 of that at 5200A.) (If much of the light in the background is caused by turbidity of the water, one may have to correct this value for the color of the suspended material. This must be determined by experiment.)

A two channel recorder would be needed to record the data. The ratio between the signals of channel one and two could be continuously calculated and the value recorded or indicated continuously - this would give a continuous record of the vertically integrated value of luminescence of rhodamine B.

It is important to note that the use of a single channel photometer centered at 5800Å may in itself be adequate, since it is only necessary to establish the reflectance level for an area free of dye. The function of the second channel at 5200Å is only to establish continuously this background level.

Table VIII

RADIANCE AND DETECTOR POWER FOR PHOTOMETER*

Dye Concentration	Spectral Radiance watt/cm^2/ster./200Å	Power on Detector Watts	S/N for S-4 s = .02 at 5200A s = .01 at 5500A	S/N for f = 6.5 cps
1PPB-10M 5800Å	18.5×10^{-6}	1.13×10^{-8}	$\frac{1.9 \times 10^4}{\sqrt{\Delta f}}$	7.5×10^3
30PPB-1M 5800Å	54.5×10^{-6}	3.3×10^{-8}	$\frac{3.2 \times 10^4}{\sqrt{\Delta f}}$	12.6×10^3
30PPB-10M 5800Å	380×10^{-6}	2.3×10^{-7}	$\frac{8.5 \times 10^4}{\sqrt{\Delta f}}$	3.3×10^4
Sky Background 5800Å	3.4×10^{-6}	2.1×10^{-9}	$\frac{8.1 \times 10^3}{\sqrt{\Delta f}}$	3.2×10^3
Sky Background 5200Å	4×10^{-6}	2.4×10^{-9}	$\frac{4 \times 10^3}{\sqrt{\Delta f}}$	1.6×10^3

*The calculated values apply to the photometer whose characteristics are given in Table VI.

The instrument in either case would be very small and compact, and could be hand held and pointed as desired for spot checks on various areas if so desired.

2.5 Other Techniques

The idea of using filters centered on the emission band at 5800Å and at a non-fluorescent region 5200Å is not restricted to the simple photometer discussed in Section 2.4 above. Many modifications are possible.

The 5800Å filter might be used in conjunction with a multispectral scanner to form an image similar to that of the photographic system, and, if necessary, a similar image formation using the 5200Å filter. The resulting picture could be compared to determine the vertically integrated amount of dye.

Another approach that might prove useful would be to form the image using an appropriate color filter with an image disector, image orthicon or vidicon using television techniques for scanning and recording the image formation.

Two image dissectors might be scanned together (one using a 5800Å filter and the other 5200Å) and the ratio of difference of the two signals used to form an image or continuously read out the amount of dye.

3. CONCLUSIONS

A number of systems for detection of rhodamine B in water have been outlined.

All systems suffer from interference from reflection of the sun by wavelets ("sun-glitter"). Imaging systems are less effected than others, since it is easy to see the areas of "sun-glitter" and neglect them in analyzing the images.

The interferometer system tends to reduce the effect of background and should prove useful for very low concentrations provided the "sun-glitter" can be reduced to a minimum; initial test runs may indicate appropriate viewing angles to avoid glitter reception. The interferometer system with its narrow band pass is the only one that can be applied to luminescence detection in general. That is, it is the only system that can be used for detection of luminescence of minerals and rocks, as well as rhodamine B or other luminescent dye, or organism where the light scattered from the material is large compared to the luminescence value.

The photographic system, while essentially similar to a filter system, requires subsequent analysis of the film by a densitometer in order to obtain the concentration.

A photometer or multispectral scanning system, or a television scanning system, would be processed electronically as the time data is taken, so as to give a read out of vertically integrated amount of dye.

Further study will be required to determine the system most useful for the particular problem.

4. REFERENCES

1. Grainger, J. F. and Ring, J., "Anomalous Fraunhofer Line Profiles," in Letter to the Editor, Nature 193, p. 762, (February 1962).

2. Ichiye, T. and Plutchak, N. B., "Photodensitometric Determination of Dye Concentration in the Ocean," Limnology and Oceanography 11, (2) 364-370 (July 1966)

3. Koller, L. R., "Ultraviolet Radiation," p. 133, J. Wiley and Sons, Second Edition (1965).

4. Kopal, Z., "Physics and Astronomy of the Moon," pp. 390-391, Academic Press (1962).

5. Poritsky, B. A., "Some Optical Properties of Fluorescent Rhodamine B," J. Franklin Institute 197, pp. 527-532 (1924).

6. Zworykin, V. K. and Ramberg, F. G., "Photoelectricity and Its Application," J. Wiley and Sons (1950)

APPENDIX A

SPECULAR REFLECTION OF DIRECT SUNLIGHT FROM WATER WAVES

The specular reflection geometry for the assumed sinusoidal water surface is shown in Figure 5. Applying the law of reflection to a single facet of the wave surface which is planar in the limit, one obtains the simple geometry of Figure A-1.

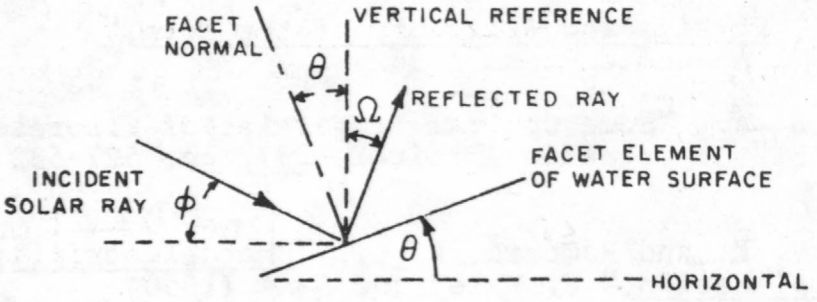

FIGURE A-1

For the facet on the water wave oriented at an angle θ from the horizontal, the solar ray coming in at an elevation angle of $\emptyset$ will be reflected at an angle, Ω, of $\pi/2 - \emptyset - 2\theta$ from the vertical. The value of θ is easily expressed for each point on the sine wave of Figure 5, which is redrawn below to include a rectangular coordinate system (Figure A-2).

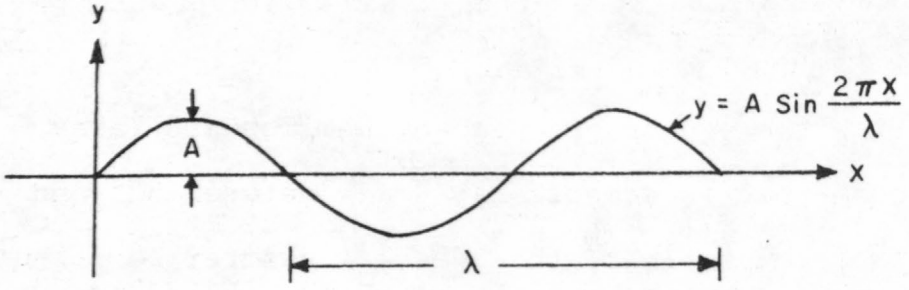

FIGURE A-2

Since the surface slope at any point on the water wave is given by

$$\frac{dy}{dx} = \tan\theta = \frac{2\pi A}{\lambda} \cos\frac{2\pi x}{\lambda} \qquad \text{(A-1)}$$

then

$$\theta = \text{Tan}^{-1}\left[\frac{2\pi A}{\lambda} \cos\frac{2\pi x}{\lambda}\right] \qquad \text{(A-2)}$$

Excluding multiple reflections between opposing faces of the water wave surface (which tends to weaken and diffuse the reflected radiation), the reflected rays come off at angles from the vertical, expressed by

$$\frac{\pi}{2} - \phi - \left| 2\text{Tan}^{-1}\frac{2\pi A}{\lambda}\right| \leq \Omega \leq \pi/2 - +\phi+ \left|2\text{Tan}^{-1}\frac{2\pi A}{\lambda}\right| \qquad \text{(A-3)}$$

For the example cited in Section 2.3.1, the solar elevation angle, ϕ, was 40° with an A/λ ratio of 0.125 (or, $\text{Tan}^{-1}\frac{2\pi A}{\lambda} \approx 38°$) so that

$$-26° \leq \Omega \leq 126°$$ (shadowing and multiple reflection restricts this to slightly less than 90°)

where the plus and minus signs of Ω correspond respectively to reflections away from and twoards the Sun, with the vertical (zenith) as angle reference.

Figure A-3 depicts the scattered-ray configuration indicated for the computed example.

By tilting the sensor acceptance beam forward (away from the Sun) such that is accepts rays, say between 35° and 45° from its platform vertical, the specular glitter component should be heavily reduced. It is noted that a lower solar

elevation angles, say 30° instead of 40° assumed previously, the minimum acceptance angle is reduced to 16° as opposed to the 26° shown in Figure A-3.

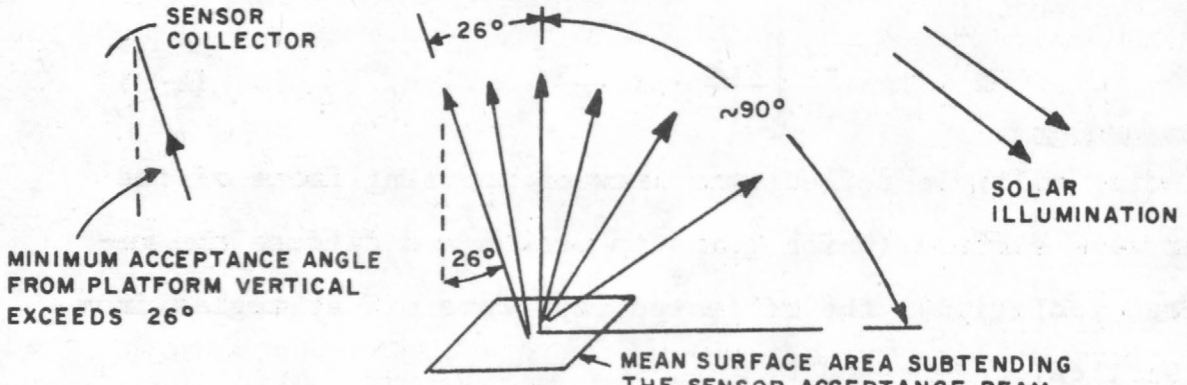

FIGURE A-3

The preceding discussion is intended solely for illustration of a possible technique that may allow use of the line-depth method under wave glitter conditions. The finer surface structure on the wave surface as well as the variety of A/λ conditions that one will encounter may radically modify the idealized ray scatter discussed in this Appendix. Although the anticipated radiance, w/cm^2-ster., from direct sun reflection is some four orders of magnitude higher than the reflected sky light (Table VI in report body) the effective area contributing to the specular reflection of sunlight may be appreciably reduced by the technique proposed. At this writing, one can only suggest that an experimental a/c program would resolve the effectiveness of this technique.

DISTRIBUTION LIST – TECHNICAL LETTERS

Dr. Richard J. Allenby (2 copies)
Deputy Director
Manned Space Science, OSSA
Code SM, NASA Headquarters
Washington, D.C. 20546

[redacted] (5 copies)
Program Chief, Earth Resources Survey
Code SAR, NASA Headquarters
Washington, D.C. 20546

Mr. A. B. Campbell
U.S. Geological Survey
Chief, Northern Rocky Mt. Branch
Bldg. 25, Federal Center
Denver, Colorado 80225

Mr. W. D. Carter
Geology Coordinator
U.S. Geological Survey
Rm. B-305, GSA Building
Washington, D.C. 20242

Mr. Leo F. Childs
Code TE-2
NASA Manned Spacecraft Center
Houston, Texas 77058

Mr. Robert L. Christiansen
Special Projects Branch
U. S. Geological Survey
Bldg. 25, Federal Center
Denver, Colorado 80225

Dr. Robert Neil Colwell
Dept. of Forestry
243 Mulford Hall
University of California
Berkeley, California 94720

John E. Cotton
U.S. Geological Survey
Water Resources Division
John F. Kennedy Federal Building
Boston, Massachusetts 02203

Max Crittenden
U.S. Geological Survey
345 Middlefield Road
Menlo Park, California 94025

John F. Cronin
Geotechnics Branch
Terrestrial Science Lab, AFCRL
Bedford, Mass. 01731

Mr. David F. Davidson
Chief, Geochemical Census
U.S. Geological Survey
Bldg. 25, Federal Center
Denver, Colorado 80225

Ralph L. Erickson
U.S. Geological Survey
Branch of Exploration Research
Denver, Colorado 80225

Mr. Raymond W. Fary, Jr. (15 copies)
Chief, RESECS
U.S. Geological Survey
801 19th Street, N.W. Room 1032
Washington, D.C. 20242

Mr. William A. Fischer (2 copies)
Research Coordinator
EROS Program/USGS
Rm. 5226 GSA Building
Washington, D.C. 20242

Forestry Remote Sensing Lab.
PSW Forest & Range Exp. Station
Box 245
Berkeley, California 94720

Dr. John C. Frye
State Dept. of Registration & Education
121 Natural Resources Building
University of Illinois Campus
Urbana, Illinois 61801

Dr. Stephen J. Gawarecki
U.S. Geological Survey
Rm. 1129 Crystal Plaza
11th Floor, Building 6
Arlington, Virginia 22202

Mr. T. George
Program Manager
Code SAB/APB & S and Aircraft Program
NASA Headquarters
Washington, D.C. 20546

(all persons receive one copy unless otherwise noted)

Dr. Arch Gerlach
Geography Coordinator
U.S. Geological Survey
Rm. 6253, GSA Building
Washington, D.C. 20242

Arthur Grantz
U.S. Geological Survey
345 Middlefield Road
Menlo Park, California 94025

Gordon Greene
U.S. Geological Survey
Crystal Plaza
11th Floor, Building 6
Arlington, Virginia 22202

Bernardo Grossling
U.S. Geological Survey
RM. 4444 Interior Building
Washington, D.C. 20240

George Gryc
U.S. Geological Survey
345 Middlefield Road
Menlo Park California 94025

John Hack
Asst. Chief Geologist
Regional Geology
U.S. Geological Survey
Rm. 4211, GSA Building
Washington, D.C. 20242

William Hemphill
U.S. Geological Survey
Rm. 1123, Crystal Plaza
11th Floor, Building 6
Arlington, Virginia 22202

Tom Hendricks
U.S. Geological Survey
Federal Center, Building 25
Denver, Colorado 80225

Mr. Allen V. Heyl
U.S. Geological Survey
Building 424
Agriculture Research Center
Beltsville, Maryland 20705

Mr. Tom Hughes
Cartography Coordinator
U.S. Geological Survey
1340 Old Chain Bridge Road
McLean, Virginia 22101

Harold L. James
Chief Geologist
U.S. Geological Survey
Geologic Division
Rm. 4243, GSA Building
Washington, D.C. 20242

John E. Johnston
U.S. Geological Survey/RESECS
Room 2230, GSA Building
Washington, D.C. 20242

Montis R. Klepper
Associate Chief Geologist
U.S. Geological Survey
Room 4244, GSA Building
Washington, D.C. 20242

Mr. Allan Kover
U.S. Geological Survey
Regional Geophysics Branch
Room 413, Blair Building
Silver Spring, Maryland 20910

Dwight M. Lemmon
Assistant Chief Geologist
Engineering Geology/USGS
Room 4214, GSA Building
Washington, D.C. 20242

Librarian
Geological Survey
Federal Center, Building 25
Denver, Colorado 80225

Librarian
U.S. Goelogical Survey
Room 1033, GSA Building
Washington, D.C. 20242

Mr. Ross B. Johnson
U.S. Geological Survey
Southern Rocky Mountains
Building 25, Federal Center
Denver, Colorado 80225

(all persons receive one copy unless otherwise noted)

Librarian
U.S. Geological Survey
Branch of Astrogeology
601 East Cedar Avenue
Flagstaff, Arizona 86002

Librarian
U.S. Geological Survey
345 Middlefield Road
Menlo Park, California 94025

Dr. Joseph Lintz, Jr.
Makay School of Mines
Reno, Nevada 89507

Paul Lowman
Goddard Space Flight Center
Code 640, NASA
Greenbelt, Maryland 20771

Dr. R.J.P. Lyon (3 copies)
Chairman Infrared Team
Geophysics Department
Stanford University
Stanforn, California 94305

Don R. Mabey
Chief, Regional Geophysics Branch
USGS/Federal Center
Denver, Colorado 80225

Jules A. MacKallor
U.S. Geological Survey
801 19th Street, N.W., Room 1032
Washington, D.C. 20242

Robert McCormick
Department of the Interior
Bureau of Mines, Room 2516
Washington, D.C. 20242

George W. Moore
U.S. Geological Survey
c/o Bureau Commercial Fisheries
Marine Laboratory
La Jolla, California

Miss Winnie Morgan (2 copies)
Reports Control Officer
Grants & Research Contracts, OSSA
Code SC, NASA Headquarters
Washington, D.C. 20546

Mr. Hal T. Morris
U.S. Geological Survey
Base Metals Branch
345 Middlefield Road
Menlo Park, California 94025

Mr. Robert H. Morris
U.S. Geological Survey
Special Projects Branch
Building 25, Federal Center
Denver, Colorado 80225

Mr. Robert M. Moxham
U.S. Geological Survey
Room 1153, Crystal Plaza
11th Floor, Building 6
Arlington, Virginia 22202

Dr. A. B. Park
Agricultural Research Service O.A.
U.S. Department of Agriculture
Washington, D.C. 20250

Dallas Peck Assistant Chief Geologist
Experimental Geology
Room 4215, GSA Building
Washington, D.C. 20242

Dr. William T. Pecora
Director, USGS
Room 5243, GSA Building
Washington, D.C. 20242

Robert W. Peplies
Chm. Department Geography & Geology
East Tennessee State University
Johnson City, Tennessee 37601

Charles Pillmore
U.S. Geological Survey
Federal Center
Denver, Colorado 80225

(all persons receive one copy unless otherwise noted)

J. G. Quade
Mackay School of Mines
Reno, Nevada 89507

Robert Reeves
U.S. Geological Survey
Room 4201 GSA Building
Washington, D.C. 20242

Edward Risley
Earth Sciences, Room 080
National Academy of Sciences
2101 Constitution Avenue, N.W.
Washington, D.C. 20418

Charles J. Robinove
U.S. Geological Survey
Water Resources Division
GSA Building - Room 2226
Washington, D.C. 20242

Leverett Ropes
Water Resources Division
U.S. Geological Survey
Federal Building
St. Paul, Minnesota

Mr. Gerald G. Schaber
U.S. Geological Survey
Branch of Astrogeology
601 East Cedar Avenue
Flagstaff, Arizona 86002

Mr. Daniel R. Shawe
U.S. Geological Survey
Light Metals & Industrial Minerals
Building 25, Federal Center
Denver, Colorado 80225

Mr. D. B. Simonett
Geography & Meterology
CRES, the University of Kansas
Lawrence, Kansas 66045

Parke D. Snaveley (2 copies)
U.S. Geological Survey
345 Middlefield Road
Menlo Park, California 94025

Mr. David L. Southwick
U.S. Geological Survey
Agriculture Research Center
Building 420
Beltsville, Maryland 20705

Ogden L. Tweto
Assistant Chief Geologist
Economic Geology/USGS
Room 4240, GSA Building
Washington, D.C. 20242

William Vest
IIT Research Institute
Suite 300
1200 17th Street, N.W.
Washington, D.C. 20036

Mr. R. E. Wallace
U.S. Geological Survey
Pacific Coast States Branch
345 Middlefield Road
Menlo Park, California 94025

Russell G. Wayland (3 copies)
USGS/Conservation
Room 3243, GSA Building
Washington, D.C. 20242

Prof. E. H. Timothy Whitten
Geology Department
Northwestern University
Evanston, Illinois 60201

Donald R. Wiesnet
U.S. Geological Survey
Water Resources Division
John F. Kennedy Federal Building
Boston, Massachusetts 02203

Mr. Edward W. Wolfe
U.S. Geological Survey
Pacific Coast Branch
345 Middlefield Road
Menlo Park, California 94025

Mr. Ed Zeitler
Code TF2
Manned Spacecraft Center
Houston, Texas 77058

Dr. Isodore Zietz
U.S. Geological Survey
Regional Geophysics Branch
Room 415, Blair Building
Silver Springs, Maryland 20910

H. J. Yatko
Manager, Spacecraft Oceanography Project
U.S. Naval Research Lab, Navaceano
Washington, D.C. 20390

NOTE: TEN (10) COPIES TO AUTHOR
OF TECHNICAL LETTER

(all persons receive one copy unless otherwise noted)